OPEN ACCESS
IOP Publishing
Superconductor Science and Technology
Supercond. Sci. Technol. **38** (2025) 035007 (11pp)
https://doi.org/10.1088/1361-6668/ada831

Development and performance of high-temperature superconducting CORC® cables with CFD REBCO tapes

Haïfa Ben Saâd[1,2,*], Christian Lacroix[1,2,*], Delano Horn-Bourque[1], Emelie Nilsson[3], Jean-François Rouquette[3], Danko van der Laan[4,5], Jeremy Weiss[4,5], Kyle Radcliff[4] and Frédéric Sirois[1,*]

[1] Polytechnique Montreal, Montreal, QC H3C 3A7, Canada
[2] Boreal Conductors Inc., Montreal, QC H2S 2P9, Canada
[3] Airbus UpNext SAS, Toulouse 31707, France
[4] Advanced Conductor Technologies LLC, Boulder, CO 80301, United States of America
[5] University of Colorado, Boulder, CO 80309, United States of America

E-mail: haifa.ben-saad@polymtl.ca, christian.lacroix@polymtl.ca and f.sirois@polymtl.ca

Received 14 August 2024, revised 23 December 2024
Accepted for publication 8 January 2025
Published 11 February 2025

Abstract

Increasing the normal zone propagation velocity (NZPV) in superconducting cables based on rare earth barium copper oxide (REBCO) tapes is expected to cause a paradigm shift by enabling the development of faster and more reliable quench detection systems to mitigate the development of destructive hot spots. Furthermore, a higher NZPV is beneficial in terms of fault current limitation capabilities by accelerating the homogenization of the quench in superconducting power devices. One way envisioned to increase the NZPV of cables based on REBCO tapes is the current flow diverter (CFD) concept. A Conductor on Round Core (CORC®) cable made with CFD REBCO tapes, called CFD CORC® cable, and a CORC® cable made with regular REBCO tapes, were fabricated and tested. The critical current of the CFD and regular CORC® cables were obtained at temperatures ranging from 67 to 77 K in self-field. Measurements showed that the NZPV was increased by a factor of 4–4.5 in the case of the CFD CORC® cable. Furthermore, the results suggest that the NZPV depends only on the applied current, similar to what has been observed previously on single REBCO tapes. These results demonstrate the successful integration of CFD REBCO tapes in CORC® cables, without compromising their superconducting properties or their enhanced NZPV. The possibility of enhancing the NZPV of REBCO-based cables could facilitate quench detection, which remains an important issue in HTS magnet applications. This advancement also holds promise for the fault current limitation functionality of CORC® cables.

Keywords: current flow diverter (CFD), quench detection, high-temperature superconductors, CORC® cables, normal zone propagation velocity (NZPV)

* Authors to whom any correspondence should be addressed.

1. Introduction

Rare earth barium copper oxide (REBCO) coated conductors (CCs) offer unprecedented performance regarding the operating temperature, current density, and applied magnetic field. For instance, these materials exhibit excellent superconducting properties above the boiling temperature of liquid nitrogen or in a magnetic field that exceeds 20 T (upper critical magnetic field of more than 100 T at 4.2 K) [1–3]. Recently, high-field magnets based on single REBCO tapes achieved a record DC magnetic field of 45.5 T, making this class of material a promising candidate for fusion and accelerator magnets [4].

In the last decade, the fusion and particle accelerator communities, such as the U.S. Magnet Development Program (MDP) [5], the European EuCARD-2 collaboration [6, 7] and the collaboration between Commonwealth Fusion Systems (CFS) and the Massachusetts Institute of Technology (MIT) [8, 9], have led several projects to develop high-field magnets manufactured from REBCO tapes and cables. These magnets require high operating currents that exceed 10 kA and low magnet inductance [10–13]. Furthermore, superconducting cables assembled from REBCO tapes have gained interest in power transmission, enabling high transmission capacity in a compact size and in some cases, fault current limitation capability [14]. REBCO cables are currently being installed and tested in the electric networks of electric navy ships [15], railway applications [16] and electric aircraft systems [17, 18], to help decarbonize transportation.

Over the years, several cabling assemblies have been proposed, including Roebel cables [19–22], Twisted-Stacked Tapes Cables (TSTC) [23–26], Symmetric Tape Round (STAR) wires [27], VIPER cables [28], and Conductors on Round Core (CORC®) cables [29]. In particular, CORC® cables have gained interest due to their round cross-section, mechanical flexibility, high current carrying capacity (up to 500 A mm^{-2} at 4.2 K and in a magnetic field of 20 T), and thermal stability [30, 31].

An interesting feature of CORC® cables is that no interlayer insulation separates the REBCO tapes, which allows for some current sharing between the tapes when a normal zone nucleates. This current redistribution in CORC® cables may provide a signal that could help detect the quench and activate a protection system to prevent a thermal runaway. Different quench detection approaches, such as optical fibers [32–34], hall probe-based technique [35], and active acoustic thermometry [36], were tested on CORC® cables. However, the efficacy of these methods for the safe operation of superconducting devices has yet to be demonstrated [37].

Until now, quench detection experiments have been conducted on CORC® cables made from regular (commercial) REBCO tapes. Regular REBCO tapes are known to have a low normal zone propagation velocity (NZPV), as well as local critical current (I_c) variations along their length [38, 39]. The combination of these two factors can produce local hot spots that are difficult to detect, exposing CORC® cables to possible irreversible damages.

It has been demonstrated that the current flow diverter (CFD) concept can increase the NZPV in REBCO tapes by a factor of 3–22 [40–42]. This concept is based on the modification of the architecture of regular REBCO tapes by inserting a non-uniform interfacial resistance (R_i) between the REBCO layer and the silver stabilizer. When a normal zone nucleates, this arrangement forces the current to take the path with the lowest resistance when it transfers from the REBCO layer to the silver layer. The deviation of the current path increases the current transfer length (CTL) between the REBCO and the silver layers, leading to an increase in the NZPV [40]. This was demonstrated experimentally on centimeter-scale REBCO tapes [41], as well as on meter-scale REBCO tapes [42].

In this paper, the performance of several CFD REBCO tapes assembled in the form of a CORC® cable, called CFD CORC® cable, is investigated. The performance of the CFD CORC® cable is compared with that of a regular CORC® cable fabricated using regular REBCO tapes. The NZPV of regular and CFD CORC® cables without copper stabilizer was measured for different applied currents and temperatures. The results are compared with the NZPV of single tapes (CFD and regular architectures) to verify whether quench propagation mechanisms remain the same when CFD and regular tapes are wound in the form of a CORC® cable. The first section includes the fabrication details of the CFD and regular CORC® cables used in this paper, along with a description of the critical current and NZPV measurements setup. The second section describes the critical current measurements performed on these CORC® cables at temperatures ranging from 67 to 77.3 K. The final section presents NZPV measurements of the CORC® cables.

2. Experimental approach

2.1. REBCO tapes parameters

Commercial REBCO tapes purchased from SuperPower Inc. (SP) were used to fabricate two CORC® cables: a first CORC® cable made with CFD REBCO tapes and a second CORC® cable made with regular REBCO tapes, which, for the rest of the paper, will be called CFD CORC® cable and 'regular' CORC® cable, respectively. Regular SP REBCO tapes, as shown in figure 1(a), contained a 50 μm thick Hastelloy substrate on which was grown a stack of oxide buffer layers having a thickness of 0.58–0.78 μm. On the buffer layers, a 1.6 μm thick REBCO layer was deposited by metal–organic chemical vapor deposition [43]. Finally, a silver stabilizer layer surrounding the 4 mm wide REBCO tape was deposited (the total thickness of silver was 2.5 μm). Interfacial resistance values between silver and REBCO layers in regular REBCO tapes are typically between 0.02–0.1 $\mu\Omega$.cm^2. Such values are obtained after annealing the tapes in an oxygen atmosphere at a temperature higher than 500 °C [44, 45].

In the CFD architecture, a patterned high interfacial resistance (CFD layer) was inserted in the central part of the tape, between the REBCO and the silver layer (see figure 1(b)). This was done by first applying an ink mask to protect the regions where a low interfacial resistance at the REBCO/silver

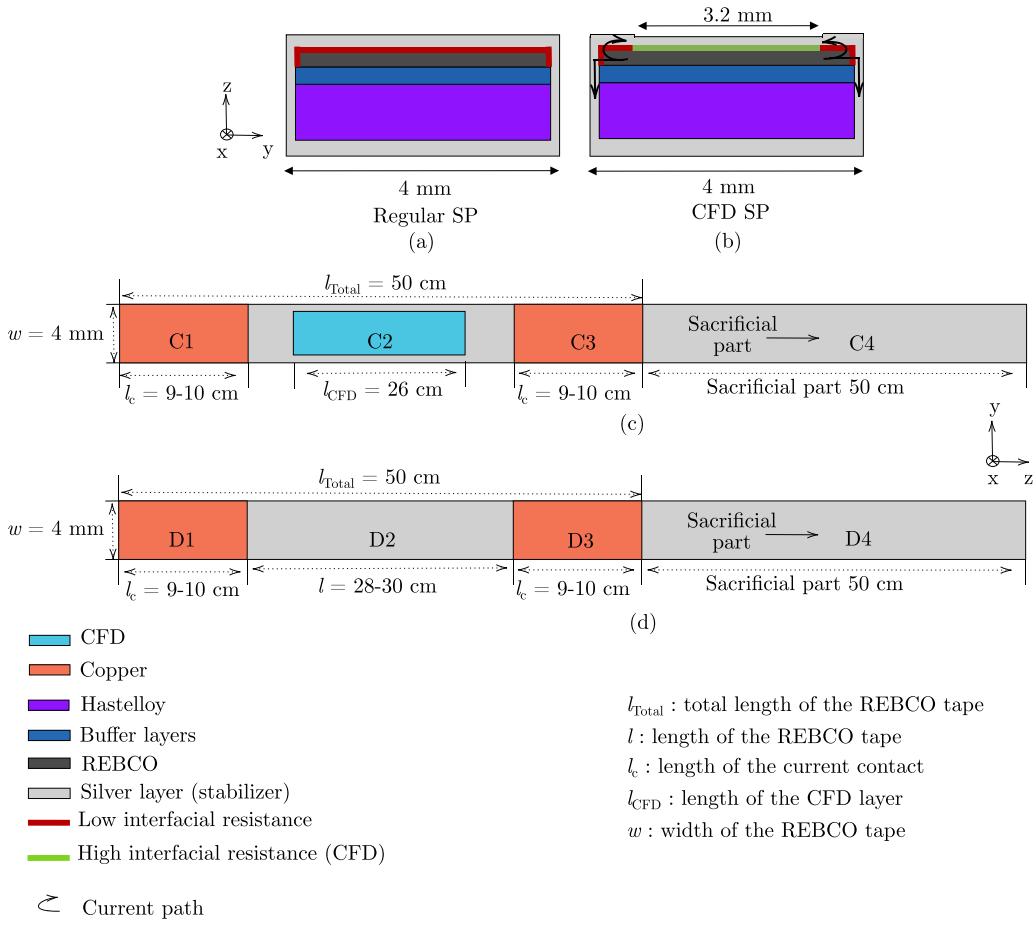

Figure 1. Geometry of the fabricated tapes to be integrated in CORC® cables: (a) cross-sectional view of the regular architecture, (b) cross-sectional view of the CFD architecture, (c) top view of the CFD SP tape, and (d) top view of the regular SP tape.

interface is needed. Then, the unprotected silver was chemically etched using an aqueous solution of peroxide (H_2O_2), ammonium hydroxide (NH_4OH), and water with a 1:1:4 dilution ratio, exposing the REBCO layer to the ambient atmosphere. Following the etching process, a thin degraded amorphous resistive layer was created at the REBCO surface [46]. In the CFD part, the value of the high interfacial resistance at the REBCO/silver interface is between 100 and 320 $\mu\Omega.cm^2$ [47]. The width of the CFD layer was 3.2 mm, which corresponds to a coverage fraction f of 0.8 (f is the ratio between the total width of the tape and the width of the CFD layer) [40].

To fabricate the CFD CORC® cable, six one-meter-long CFD tapes were first manufactured using custom reel-to-reel machines. The fabrication steps that have been automated include the masking step, the chemical etching step, the unmasking step, and the cleaning step on meter-scale REBCO tapes. In the masking reel-to-reel setup, an ink dispenser applies a masking coating to protect regions where a low interfacial resistance is required. Afterward, the REBCO tapes are transferred in the reel-to-reel etching and unmasking setup, before finally proceeding to silver deposition. Further details about the reel-to-reel CFD fabrication process are available in [42]. Figure 1(c) illustrates the top view of the geometry of the CFD REBCO tapes. Each tape comprised four different sections over its length, named C1, C2, C3, and C4. Sections C1 and C3 (orange rectangles) were dedicated to the CORC® cable terminals. In these sections, 10 μm of copper was electrodeposited locally over a length of $l_c = 9 - 10$ cm on each side of the tape to facilitate the indium soldering of the CORC® cable terminals without destroying the silver layer. Indeed, soldering with indium on a thin silver layer creates an intermetallic compound indium-silver (In–Ag) on top of the REBCO layer [47, 48]. In the worst case, the silver layer can be completely consumed, and the solder may react with the REBCO layer, leading to a degradation of the critical current. The CFD layer was integrated into section C3 (cyan rectangle) over a length $l_{CFD} = 26$ cm. Section C4 consists of a 50 cm long sacrificial part, which is required to attach the tape to the CORC® cable winding machine. Once the tapes are wound around the core, this sacrificial part is removed.

Six one-meter-long regular SP tapes were also prepared to manufacture a 30 cm long regular CORC® cable. Figure 1(d) illustrates the top view of the geometry of the regular REBCO tapes used to fabricate the regular CORC® cable. Similarly to the CFD tapes, the regular REBCO tapes contained four

Table 1. Main parameters of the CFD and regular REBCO tapes.

Parameters	CFD tape	Regular tape
Width (mm)	4	4
Top silver layer thickness (μm)	1	1
Bottom silver layer thickness (μm)	1.5	1.5
I_c at 77 K, self field (A)	120 ± 4	123 ± 3
n at 77 K, self field	22 ± 2	21 ± 2
Thickness of the tape e (μm)	55	55
CFD coverage fraction f	0.8	0

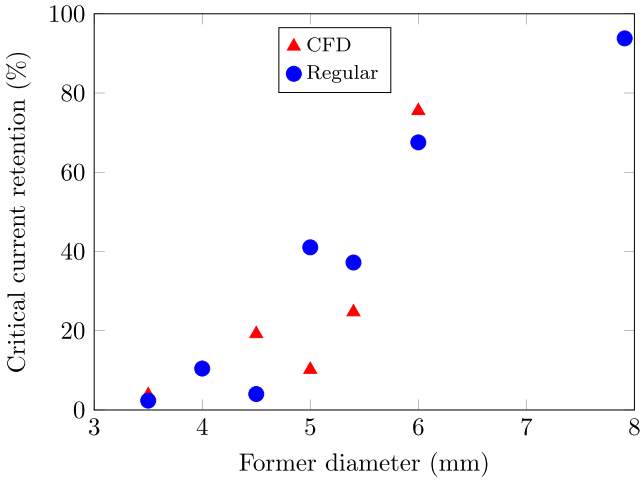

Figure 2. Critical current retention of CFD REBCO tapes (red triangle) and regular REBCO tapes (blue circles), after being bent at an angle of approximately 45° on copper formers with various diameters.

sections, named D1, D2, D3, and D4, where sections D2 and D4 (grey rectangles) remained unmodified, and sections D1 and D3 (orange rectangles) were copper-coated for the current terminals of the cable. Table 1 gives the main parameters of the CFD and regular REBCO tapes employed to fabricate the CFD and regular CORC® cables, respectively.

2.2. CORC® cable parameters

Before the fabrication of the CORC® cables, bending tests were performed on the CFD and regular REBCO tapes to determine the minimum former diameter on which both CFD and regular tapes could be wound without degradation of their critical current. REBCO tapes were wound with the superconducting layer facing the former, resulting in the REBCO layer experiencing axial compressive strain. REBCO tapes typically withstand over -1% of axial compressive strain without significant performance degradation [13]. Figure 2 shows the critical current retention as a function of the former diameter for CFD REBCO tapes (red triangles) and regular REBCO tapes (blue circles). Results showed that the critical current was reduced by 25% for the CFD tape, and by 32% for the regular tape, when the tapes were bent around a diameter of 6 mm. Therefore, a copper former of 6.35 mm OD, was used to fabricate the CORC® cables, on which two layers of thermoplastic (heat shrink) were added to electrically insulate the REBCO tapes from the former, resulting in an overall bending diameter of 6.9 mm.

The CFD and regular CORC® cables contained two layers of REBCO tapes. The two layers were wound in opposite directions, with no additional material introduced between them. In one layer, three REBCO tapes were twisted, with the REBCO surface facing the insulated copper former. The winding angle was 38.6° for the inner layer, and 37.7° for the outer layer. Figure 3 shows an example of the fabricated CORC® cables. Both ends of the CORC® cables were inserted in copper tubes with an ID of 9.4 mm and an OD of 12.7 mm. The copper tubes were then filled with indium solder to ensure a good electrical contact between the tapes and the copper tube. The terminal length was 4 cm for the CFD CORC® cable and 3 cm for the regular CORC® cable. The parameters of both cables are presented in table 2. A schematic representative of a CORC® cable is presented in figure 4.

2.3. Critical current and NZPV measurements

Figure 5 displays a picture of the sample holder and voltage measurement system used in this work. The sample was connected to the power supply with copper cables screwed in copper blocks fixed to the CORC® cable terminations. Cylindrical grooves were made in the copper blocks to match the shape of the CORC® cable terminations. Each cable termination was

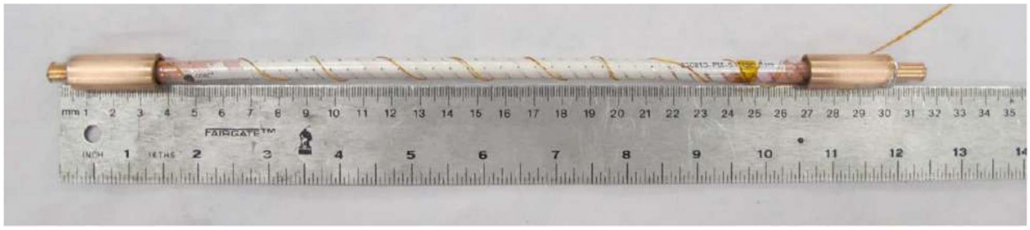

Figure 3. CORC® cable containing two layers. Three REBCO tapes were twisted in each layer facing the copper former.

Table 2. Main parameters of the CFD and regular CORC® cables.

Parameters	CFD CORC®	Regular CORC®
Total cable length (cm)	30	30
Number of layers	2	2
Number of tapes per layer	3	3
Terminals length (cm)	4	3
Terminals diameter (mm)	12.7 (OD), 9.4 (ID)	12.7 (OD), 9.4 (ID)
Copper former radius R (mm)	3.45	3.45
Twist pitch of the outer layer t (mm)	17	17
Winding angle of outer layer β (°)	37.7	37.7
Former-tape insulation	Thermoplastic	Thermoplastic

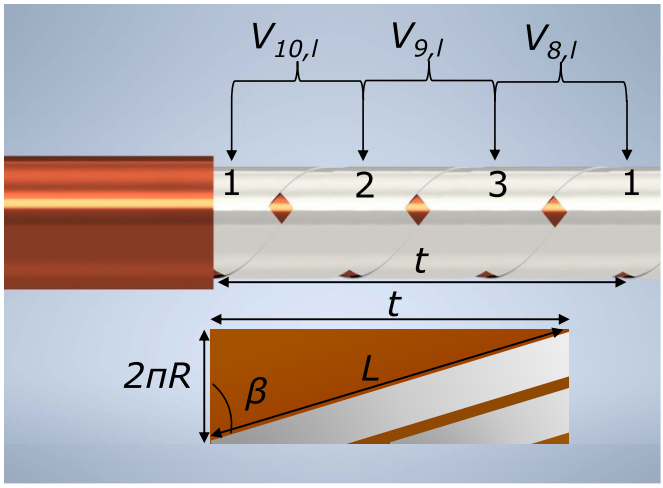

Figure 4. Top figure: schematic of the position of the voltage taps ($V_{i,l}, i = 10, 9, 8, l =$ left) on the outer layer of the CORC® cable. Bottom figure: schematic of REBCO tapes in a CORC® cable in a rectangular plane showing the length L of a straight piece of REBCO tape along a full twist pitch t, and the twist angle of the outer layer β.

securely screwed between the two copper blocks to ensure a balanced current injection. The sample and copper blocks were installed on a wooden support but not anchored to avoid damage due to thermomechanical constraints during cooling. During measurements, the entire assembly was immersed in a liquid nitrogen bath.

For the electrical measurements, a pulsed current source was used to inject square pulse currents of various amplitudes in the cables. The I_c was determined by measuring the total voltage over the entire cable and by using an electric field criterion (E_c) of 1 μV cm^{-1}. The total voltage was measured from two voltage taps soldered inside the CORC® cable terminals, with a tap dedicated to each terminal.

A 16 cm long printed circuit board (PCB) with pogo pins soldered at every 5.9 mm, used as voltage taps, was used to measure the NZPV. The distance between each pogo pin was based on the twist pitch of the cables, which ensured that each pogo pin was positioned in the middle of each tape on the outer layer, as shown in figure 4(top). Pogo pins thus measured the potential difference ($V_{i,l}$, $i = 10$, 9 and 8 in figure 4) between two adjacent tapes on the outer layer. The measured voltages were recorded by a multi-channel data acquisition card (DAQ). To initiate a quench, cylindrical NdFeB magnets were inserted in the wooden support to decrease locally the critical current of the CORC® cable over a length of 8 mm (see figure 5(d)).

To perform temperature-dependent measurements, the CORC® cable and its sample holder were installed in a closed cryostat containing liquid nitrogen, and in which the pressure was reduced with a vacuum pump to reduce the boiling point of the liquid nitrogen and decrease its temperature. This method enabled us to perform measurements at any temperature between 65 and 77 K. Within the cryostat, PT100 sensors were employed to monitor the temperature. The sensors were installed at different height levels in the cryostat (4 cm, 8 cm, and 12 cm) to monitor the temperature. No significant temperature gradient was observed between the sensors, i.e. the differences measured being within $\pm$0.05 K. A capacitive level sensor was used to measure the liquid nitrogen level during measurements, to make sure the sample remained in liquid nitrogen during the entire experiment.

3. Critical current measurements

Before the fabrication of the CORC® cables, the critical currents of the CFD and regular REBCO tapes dedicated to the cables were measured in liquid nitrogen at ambient pressure (77 K) and in self-field. Figure 6 presents measurements of the

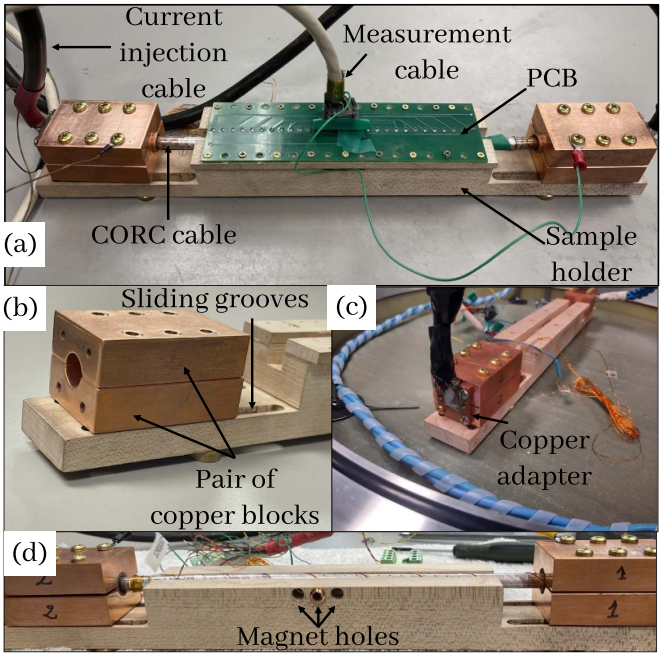

Figure 5. Sample holder and voltage measurement system used to obtain the critical current and the NZPV. The PCB has pogo pins on the hidden side that are used as electrodes for the voltage taps. (a) Example of a CORC® cable installed in the sample holder. (b) Copper blocks between which the CORC® cable terminals were clamped to ensure a good current injection. (c) Rectangular copper adapter that connects the current injection cable to the copper blocks. (d) Holes were created in the sample holder to insert NdFeB magnets during NZPV measurements.

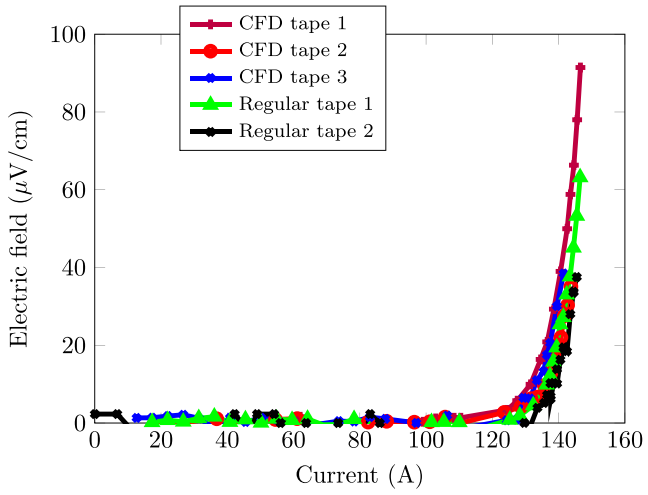

Figure 6. *E–I* curves of three CFD REBCO tapes and two regular REBCO tapes used to fabricate both CORC® cables. The measurements were performed at 77 K and in self-field before integrating the tapes into the cables.

E–I characteristics of three CFD tapes and two regular tapes prepared for the CORC® cables fabrication. The average value of the critical currents of the CFD tapes was 120 ± 4 A at an electric field criterion of 1 μV cm^{-1}, while the n-value was 22 ± 2. For the regular tapes, the average critical current was 123 ± 3 A, while the n-value was 21 ± 3.

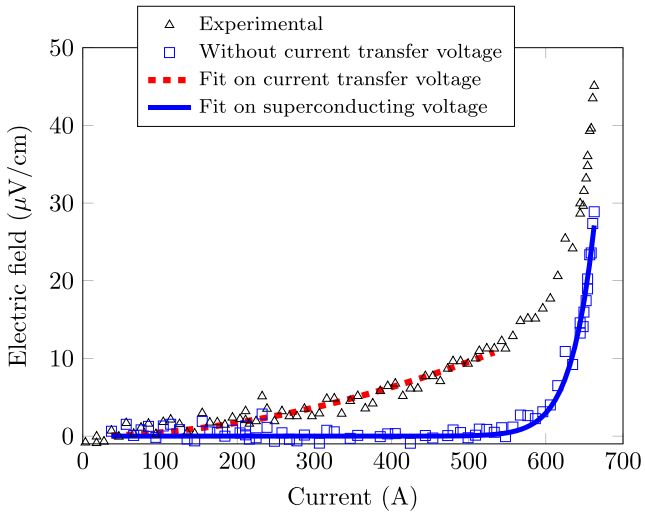

Figure 7. *E–I* curve of the CFD CORC® cable at 77 K and in self-field. The black triangles correspond to the measured electric field. The dashed red line is a fit of the current transfer voltage at low currents. Blue squares correspond to the remaining electric field after removing the current transfer voltage from the terminals over the whole range of current according to equation (1). The solid blue line is a fit of the electric field of the superconductor alone using a power law model. Using a criterion of $E_c = 1$ μV cm^{-1}, a I_c of 581 ± 4 A and a n-value of 26 ± 4 were found.

Considering the average critical current of a single tape at 77 K in self-field and ignoring any self-field effects in the cable, the nominal critical current of the CORC® cables was determined by multiplying the average tape I_c by the number of tapes (6), giving a nominal I_c of 720 A for the CFD CORC® cable, and 738 A for the regular CORC® cable.

Before performing critical current experiments on the CORC® cables, the room temperature resistance was measured using the voltage taps inserted in the terminals. Values of 52 mΩ for the CFD CORC® cable and 44 mΩ for the regular CORC® cable were obtained.

The *E–I* curve of the CFD CORC® cable was first measured at 77 K (black triangles in figure 7). At low currents, a voltage originating from the current transfer from the cable terminals to the superconductor can be observed. Using the baseline method [44], this contribution can be subtracted from the experimental data to obtain the electric field of the superconductor alone. A power law function was used to fit the experimental data at low currents. The electric field in the superconductor E_s is thus given by:

$$E_s = E - E_c \left(\frac{I}{I_{c,r}} \right)^{n_r}, \qquad (1)$$

where $E_c = 1$ μV cm^{-1} , $I_{c,r}$ and n_r (the index r refers to the resistive current transfer voltage) are variables that were adjusted for the fit (red dashed line in figure 7). Values of 150 A and 1.9 were found respectively for $I_{c,r}$ and n_r.

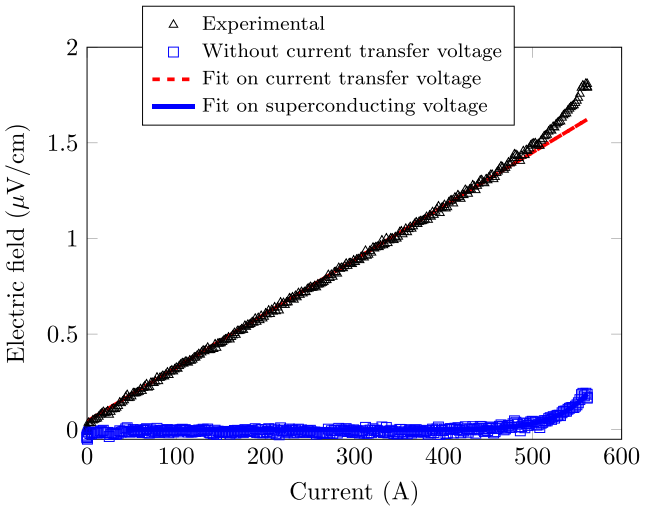

Figure 8. *E–I* curve of the regular CORC® cable at 76 K and in self-field. The black triangles correspond to the measured electric field. The dashed red line is a linear fit of the current transfer voltage at low currents. Blue squares correspond to the remaining electric field after removing the current transfer voltage from the terminals over the whole range of current. The solid blue line is a fit of the electric field of the superconductor alone using a power law model. Using a criterion of $E_c = 1\ \mu\mathrm{V\,cm^{-1}}$, a I_c of 629 ± 0.6 A and a n-value of 15 ± 0.4 were found.

Once the current transfer voltage is removed, the resulting data correspond to the blues squares in figure 7. These data were then fitted with a power law function (blue line). Using an electric field criterion of $1\ \mu\mathrm{V\,cm^{-1}}$, a critical current of 581 ± 4 A and an n-value of 26 ± 4 were found. We note that the critical current is 19% lower than the nominal critical current of 720 A estimated earlier. The difference between the nominal I_c and the measured I_c is probably due to a reduction in the critical current due to the magnetic field produced by the tapes on each other, or to the I_c degradation due to the strain induced in the tapes when bending them around the former [49].

For the regular CORC® cable, the critical current was measured at 76 K using the measurement setup described in [50]. In this setup, a DC ramp current was applied, and the voltage was measured using a nanovoltmeter. Figure 8 depicts the *E–I* curves obtained at 76 K of the regular CORC® cable. Values of 356 A and 1 were used respectively for $I_{c,r}$ and n_r to represent the resistive slope. A critical current of 629 ± 0.6 A and a n-value of 15 ± 0.4 were found using an electric field criterion of $1\ \mu\mathrm{V\,cm^{-1}}$, after subtracting the current transfer voltage. A calibrated sample was used to determine a conversion factor between 76 K and 77 K. The critical current of the calibration sample was first measured in a liquid nitrogen bath having a temperature of 76 K in Boulder, Colorado U.S.A., and a value of 505 A was obtained. The same sample was remeasured in a liquid nitrogen bath at 77 K in Montreal, Canada, and a I_c of 439 A was obtained, resulting in a conversion factor of 1.15, close to the value of 1.18 that was obtained in [15]. Using this conversion factor, a I_c of 546 A was obtained for the regular CORC® cable at 77 K, which is 26% lower than the nominal critical current of 738 A.

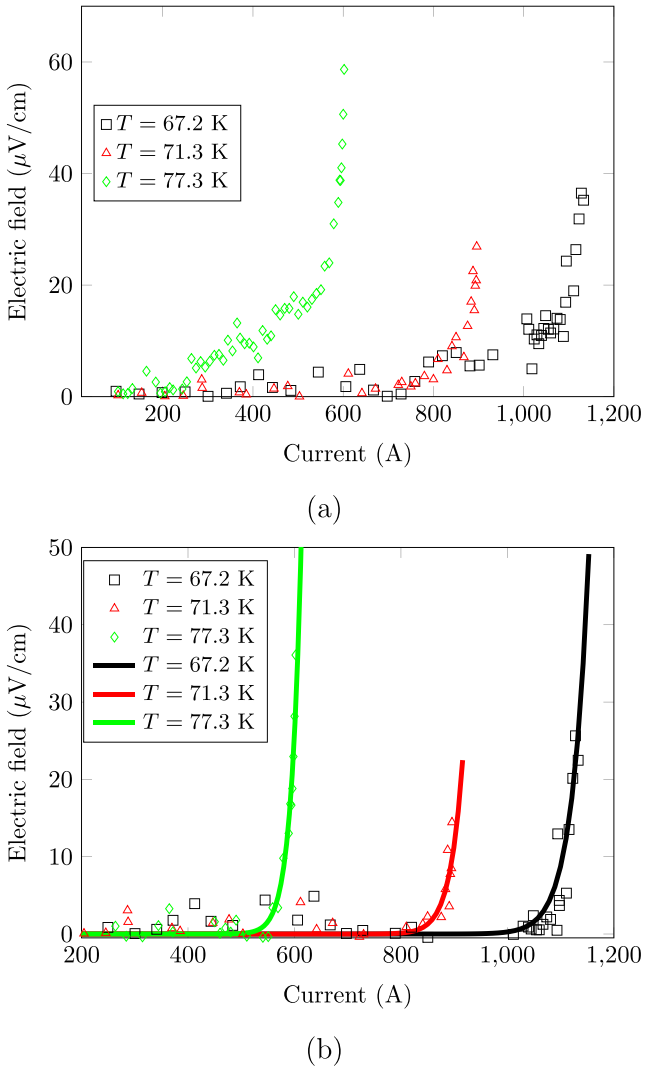

Figure 9. (a) *E–I* curves of a CFD CORC® cable as measured at temperatures T of 67.2 K, 71.3 K, and 77.3 K. (b) Same *E–I* data without the current transfer voltage, at temperatures T of 67.2 K, 71.3 K, and 77.3 K. The solid lines are a curve fitting based on a power law model.

The critical current of the CFD CORC® cable was measured at different temperatures. Figure 9 depicts the *E–I* curves obtained at 67.2 K, 71.3 K and 77.3 K. Experimental data of the *E–I* curves are presented in figure 9(a), while figure 9(b) shows the resulting *E–I* characteristics after subtracting the current transfer voltage. The solid lines represent curve fittings with a power law model.

Figure 10 presents the variation of the critical current ($E_c = 1\ \mu\mathrm{V\,cm^{-1}}$) vs. the temperature for the CFD CORC® cable. The critical current increases from 540 ± 5 A to 1031 ± 7 A when the temperature decreases from 77.3 to 67.2 K. The temperature dependence of the critical current is linear, which is consistent with previous measurements performed on single tapes and CORC® cables at low temperatures (40–77 K) [49]. The n-value was found to remain approximately constant ($\approx 33 \pm 4$) for this temperature range. We note that this n-value is much higher than that of single REBCO tapes ($\approx 22 \pm 2$).

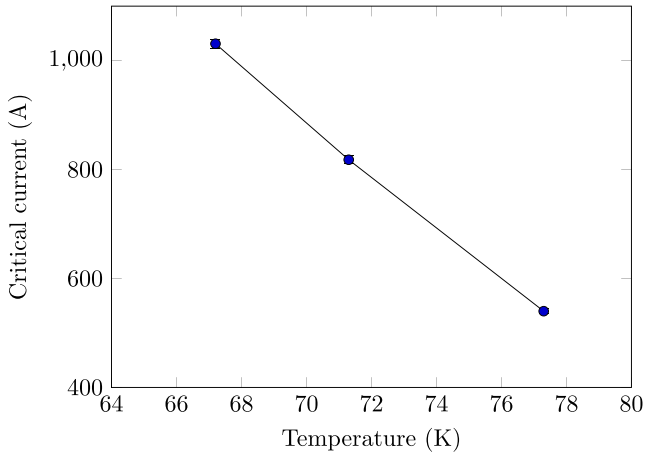

Figure 10. Temperature dependence of the critical current of the CFD CORC® cable (blue circles).

Although the reason behind this sharp transition is not clear, previous measurements performed on CORC® cables between 40 and 77 K reported a high n-value, up to 50 [13, 49].

Note that the I_c of the CFD CORC® cable at 77.3 K was slightly lower than that obtained in the initial measurement at 77 K (shown in figure 7) (540 A vs 581 A). Local measurements indicated that the voltage appeared in one of the terminals, suggesting that a degradation occurred in this terminal. It is suspected that this degradation is probably related to a bad current transfer due to the short length of the terminals. The use of longer terminals could probably solve this issue.

Unfortunately, the temperature dependence of the critical current of the regular CORC® cable could not be determined experimentally because the sample was degraded during NZPV measurements (see below). However, it is reasonable to assume that its critical current will depend on the temperature in a similar manner than the CFD CORC® cable, which would give a critical current of 1044 A at 67.2 K.

4. NZPV measurements

As described in section 2.3, the NZPV was measured using voltage taps placed at every 5.9 mm. Figure 11 presents the measured voltage that rises upon a quench in the regular CORC® cable immersed in a liquid nitrogen bath at ambient pressure (77 K), for an applied current of 590 A. The same NZPV measurement process was then repeated for applied currents ranging from 300 to 1200 A. Each $V_{i,l}(i = 1,2,3)$ (solid lines) represents the potential difference between the voltage taps placed on the left side of the quenched zone, while $V_{i,r}(i = 1,2,3)$ (dashed lines) stands for the potential difference between the taps on the right side of the quenched zone. We observe that the generated voltage upon a quench is symmetric relative to the defect, indicating that the normal zone propagates similarly in both directions. The voltage is highest at the probes that are the closest to the defect zone, and decreases as we move away from the defect. When the cable

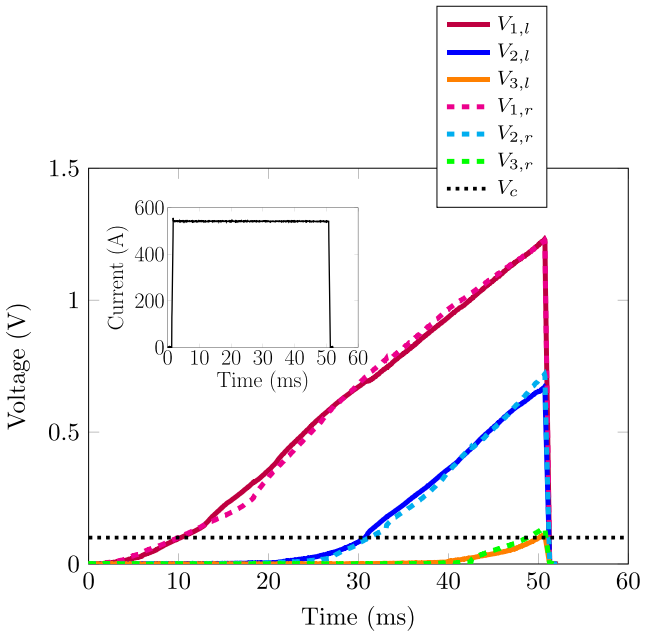

Figure 11. Measured voltage vs time during the propagation of the normal zone in the regular CORC® cable immersed in a liquid nitrogen bath at ambient pressure (77 K). Solid lines represent the voltage measured in the voltage taps ($V_{i,l}\,(i = 1,2,3)$) placed on the left side of the quench initiation zone. Dashed lines represent the voltages measured in the taps ($V_{i,r}$ $(i = 1,2,3)$) placed on the right of the quench initiation zone. The dotted black line is the voltage criterion (V_c) used to calculate the NZPV. Inset: applied current vs time (590 A lasting 49 ms).

is superconducting, the interpretation of the local voltages in CORC® cables is not obvious because of the current sharing between the tapes. However, when all REBCO tapes are quenched, the entire current flows in the stabilizer layers and the current distribution in the CORC® cable becomes homogeneous, allowing us to measure the NZPV [51, 52]. Thus, the NZPV was calculated in the conventional way, that is, by dividing the distance between two successive voltage taps by the time required to reach $V_c = 0.1$ V at both taps as follows:

$$\mathrm{NZPV} = \frac{\Delta l}{\Delta t}, \tag{2}$$

where Δl is the distance between two successive voltage taps, and Δt is the time required to reach V_c at both taps.

The NZPV of the CFD CORC® cable and of the regular CORC® cable was first obtained at 77 K and in self-field. Figure 12 presents the NZPV obtained from the propagation of the normal zone for both CORC® cables. Similar to the quench behavior of a single REBCO tape, the NZPV increases with the applied current. Furthermore, the NZPV of the CFD CORC® cable is higher by a factor of 4–4.5 compared to the NZPV of a regular CORC® cable.

It is interesting to compare the behavior of CORC® cables with that of single REBCO tapes. To make a fair comparison, the NZPV of the single REBCO tapes was divided by the ratio (p) between the initial length of the straight REBCO

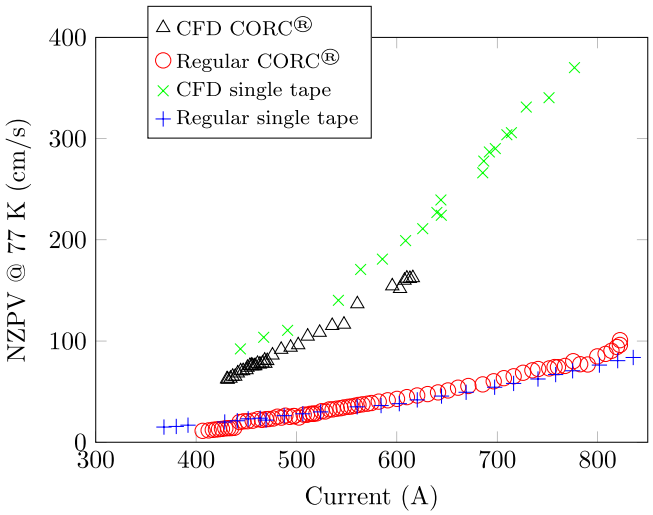

Figure 12. NZPV obtained at 77 K in self-field versus applied current for the CFD CORC® cable (black triangles), and the regular CORC® cable (red circles). The NZPV of a CFD tape (green (×) and a regular tape (blue +) divided by the length ratio p are also shown. For comparison, the applied current applied on the single tapes was multiplied by a factor of six, i.e. the number of tapes in the CORC® cables.

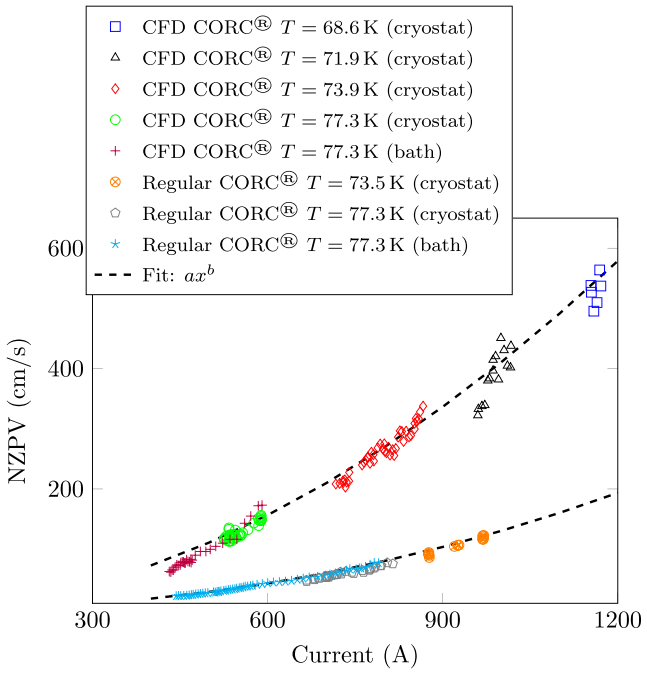

Figure 13. Experimental NZPV obtained at temperatures ranging from 68 K to 77 K in self-field vs the applied current. Dashed lines are power law functions in the form of $y = ax^b$ fitted to the experimental data. Values of $a = 9.10^{-4}$ and $b = 1.89$ were found for the CFD CORC® cable, while values of $a = 4.10^{-5}$ and $b = 2.17$ were found for the regular CORC® cable.

tape (L) and the twist pitch (t). This adjustment thus takes into account the helicoidal arrangement of the tapes in the cable. Figure 4 (bottom) presents a two-dimensional projection of the geometry of a CORC® cable in a rectangular plane. This projection was used to calculate p between the length of a straight REBCO tape and wounded tape in the CORC® cable as follows [53]:

$$p = \frac{L}{t} = \frac{1}{\sin(\beta)}, \tag{3}$$

$$t = 2\pi \tan(\beta)(R + e), \tag{4}$$

where t is the twist pitch of the outer layer, β is the winding angle of the outer layer, R is the radius of the former, L is the initial length of the straight REBCO tape over a full twist pitch, which was equal to 27 mm in our case, and e is the thickness of the tape. The p value for our CORC® cables was 1.6.

Furthermore, the current applied on the single tapes was multiplied by six, to consider that the CORC® cables contain a total of 6 tapes. In figure 12, we observe that the NZPV values for a given architecture (regular or CFD) all follow the same curve. We conclude that the geometrical arrangement of the tapes in the configuration of a CORC® cable does not affect the NZPV gain factor that we observe on individual CFD tapes.

The temperature dependence of the NZPV was measured at temperatures ranging from 68.6 K to 77.3 K (see figure 13). NZPV measurements performed in the cryostat were first made at 77.3 K to make sure that we obtained the same results as those obtained in a liquid nitrogen bath.

The dependence of the NZPV on the applied current could be well-fitted with a power law function. The parameters of the power law functions were obtained by fitting the experimental results presented in figure 13 as follows:

$$\mathrm{NZPV}_{\mathrm{CFD}}(I) = 9.10^{-4} I^{1.89}, \tag{5}$$

$$\mathrm{NZPV}_{\mathrm{regular}}(I) = 4.10^{-5} I^{2.17}. \tag{6}$$

These results suggest that the NZPV primarily depends on the applied current rather than the temperature. This is consistent with previous results found for single REBCO tapes [54, 55].

Unfortunately, the regular CORC® cable was degraded after measuring the NZPV at 73.5 K (see figure 14). The degradation occurred at the magnet location. Indeed, because of the slow NZPV, longer pulses had to be used to obtain reliable values. For example, at 77 K and for an applied current of 500 A, the pulse duration required to properly measure the NZPV was 29 ms for the CFD CORC® cable, and 59 ms for the regular CORC® cable. This increased the temperature at the magnet location to much higher values than in the case of the CFD CORC® cable.

5. Conclusion

A CFD CORC® cable was successfully manufactured by assembling six CFD REBCO tapes (two layers, three tapes per layer). The performance of the CFD CORC® cable was

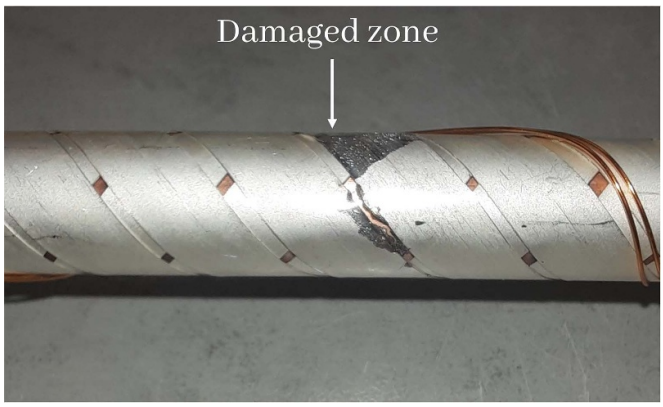

Figure 14. Damaged zone at the magnet location in the regular CORC® cable. The damage occurred during NZPV measurements.

compared with that of a regular CORC® cable, manufactured using six regular REBCO tapes. The critical current of the CFD CORC® cable at 77.3 K was 581 A, slightly higher than the critical current of the regular CORC® cable (546 A). A critical current of 1031 A was obtained at 67.2 K for the CFD CORC® cable.

Measurements showed that the NZPV of the CFD CORC® cable is 4–4.5 times higher than that of the regular CORC® cable. Furthermore, it was shown that the quench behaviors of the CFD and regular CORC® cables are similar to the behavior of single CFD and regular REBCO tapes, considering a helical longitudinal quench propagation along the tape. Also, the results suggest that the NZPV of CORC® cables depends only on the applied current and not the temperature, in agreement with previous results on the NZPV of single REBCO tapes. This suggests that in regular and CFD CORC® cables, where the tapes are electrically insulated from the copper core, the NZPV is primarily influenced by the NZPV of the individual tapes comprised in the cable. No degradation in the superconducting properties of the CFD CORC® cable was observed during the quench experiments. On the other hand, the regular CORC® cable was burnt at the magnet location.

Finally, the successful incorporation of the CFD tape architecture in CORC® cables was achieved. The gain factor of the NZPV could be further improved by adequately adjusting the CFD tape architecture itself (improvements up to 20 times have been reported on short samples [42]). While it would be beneficial to have a NZPV of the same order of magnitude as that of low temperature superconductors, increasing the NZPV of REBCO tapes by a factor of 4.5 is already a notable achievement. This is particularly interesting given that voltage detection schemes rely on the size of the normal zone, which is proportional to the voltage developed at the terminals of the device. Beyond quench detection, the results are also promising to improve the robustness of superconducting power transmission cables with fault current limitation capabilities, given that improving the NZPV homogenizes the quench in the tape, which results in better limitation dynamics and reduces local temperature gradients, known to deteriorate tapes performance.

Data availability statement

All data that support the findings of this study are included within the article (and any supplementary files).

Acknowledgments

This project has received funding from the Canadian National Sciences and Engineering Research Council (NSERC), Mitacs, and CMC Microsystems. Part of the work was also supported by the U.S. Department of Energy, Office of High Energy Physics under Contract Number DE-SC140009, and ARPA-E under Contract Number DE-AR0001459. This work has also been supported by La direction Générale de l'Aviation civile (DGAC).

ORCID iDs

Haïfa Ben Saâd https://orcid.org/0000-0002-1620-5364
Christian Lacroix https://orcid.org/0000-0002-1648-1879
Delano Horn-Bourque https://orcid.org/0009-0009-9894-0378
Emelie Nilsson https://orcid.org/0000-0002-7438-9448
Jean-François Rouquette https://orcid.org/0000-0003-2409-3881
Danko van der Laan https://orcid.org/0000-0001-5889-3751
Jeremy Weiss https://orcid.org/0000-0003-0026-3049
Kyle Radcliff https://orcid.org/0009-0002-6389-2176
Frédéric Sirois https://orcid.org/0000-0003-0372-9449

References

[1] Zhang Y, Lehner T F, Fukushima T, Sakamoto H and Hazelton D W 2014 *IEEE Trans. Appl. Supercond.* **24** 7500405
[2] Trociewitz U P, Dalban-Canassy M, Hannion M, Hilton D K, Jaroszynski J, Noyes P, Viouchkov Y, Weijers H W and Larbalestier D C 2011 *Appl. Phys. Lett.* **99** 202506
[3] Larbalestier D, Gurevich A, Feldmann D M and Polyanskii A 2001 *Nature* **414** 368–77
[4] Hahn S *et al* 2019 *Nature* **570** 496–9
[5] Gourlay S A, Prestemon S O, Zlobin A V, Cooley L and Larbalestier D 2016 The us magnet development program plan *Technical Report* (Lawrence Berkeley National Lab. (LBNL)
[6] Kirby G *et al* 2016 *IEEE Trans. Appl. Supercond.* **26** 4003307
[7] Rossi L *et al* 2014 *IEEE Trans. Appl. Supercond.* **25** 4001007
[8] Hartwig Z S *et al* 2023 *IEEE Trans. Appl. Supercond.* **25** 0600316
[9] Creely A *et al* 2020 *J. Plasma Phys.* **86** 865860502
[10] Bruzzone P, Fietz W H, Minervini J V, Novikov M, Yanagi N, Zhai Y and Zheng J 2018 *Nucl. Fusion* **58** 103001
[11] Wang X, Gourlay S A and Prestemon S O 2019 *Instruments* **3** 62
[12] Uglietti D 2019 *Supercond. Sci. Technol.* **32** 053001
[13] Van der Laan D C, Weiss J D and McRae D 2019 *Supercond. Sci. Technol.* **32** 033001
[14] Yazdani-Asrami M, Seyyedbarzegar S, Sadeghi A, de Sousa W T and Kottonau D 2022 *Supercond. Sci. Technol.* **35** 083002

[15] Van Der Laan D, Weiss J, Kim C, Graber L and Pamidi S 2018 *Supercond. Sci. Technol.* **31** 085011
[16] Allais A *et al* 2024 *IEEE Trans. Appl. Supercond.* **34** 4802207
[17] Ybanez L, Colle A, Nilsson E, Berg F, Galla G, Tassisto M, Rivenc J, Kapaun F and Steiner G 2022 Ascend: the first step towards cryogenic electric propulsion *IOP Conf. Ser.: Mater. Sci. Eng.* 1241 012034
[18] Nilsson E *et al* 2023 *IEEE Trans. Appl. Supercond.* **34** 4801704
[19] Cavallucci L, Breschi M, Ribani P L, Zhang Q and Yang Y 2021 *Supercond. Sci. Technol.* **34** 105002
[20] Otten S, Kario A, Demenčik E, Nast R and Grilli F 2020 *Supercond. Sci. Technol.* **33** 094013
[21] Pelegrin J, Bailey W and Yang Y 2021 *IEEE Trans. Appl. Supercond.* **31** 1–5
[22] Goldacker W, Grilli F, Pardo E, Kario A, Schlachter S I and Vojenčiak M 2014 *Supercond. Sci. Technol.* **27** 093001
[23] Kang R, Uglietti D and Song Y 2020 *Cryogenics* **106** 103037
[24] Celentano G, Vannozzi A, De Marzi G, Marchetti M, Augieri A, Di Zenobio A, Fabbri F, Muzzi L, Rufoloni A and della Corte A 2019 *IEEE Trans. Appl. Supercond.* **29** 1–5
[25] Liu Y and Gao Y 2024 *Supercond. Sci. Technol.* **37** 105001
[26] Takayasu M, Mangiarotti F J, Chiesa L, Bromberg L and Minervini J V 2012 *IEEE Trans. Appl. Supercond.* **23** 4800104
[27] Kar S, Sandra J S, Luo W, Kochat M, Jaroszynski J, Abraimov D, Majkic G and Selvamanickam V 2019 *Supercond. Sci. Technol.* **32** 10LT01
[28] Hartwig Z S *et al* 2020 *Supercond. Sci. Technol.* **33** 11LT01
[29] Van der Laan D, Weiss J, Noyes P, Trociewitz U, Godeke A, Abraimov D and Larbalestier D 2016 *Supercond. Sci. Technol.* **29** 055009
[30] Weiss J D, Mulder T, ten Kate H J and van der Laan D C 2016 *Supercond. Sci. Technol.* **30** 014002
[31] CORC® Cables & Wires Advanced Conductor Technologies LLC (available at: www.advancedconductor.com/corccable/) (Accessed on February 2023)
[32] Hu Z, Jiang J, Sheng J and Jin Z 2024 *Supercond. Sci. Technol.* **37** 115001
[33] Van Der Laan D, Weiss J, Scurti F and Schwartz J 2020 *Supercond. Sci. Technol.* **33** 085010
[34] Scurti F, Weiss J, Van Der Laan D and Schwartz J 2021 *Supercond. Sci. Technol.* **34** 035026
[35] Weiss J, Teyber R, Marchevsky M and Van Der Laan D 2020 *Supercond. Sci. Technol.* **33** 105011
[36] Marchevsky M, Hershkovitz E, Wang X, Gourlay S A and Prestemon S 2018 *IEEE Trans. Appl. Supercond.* **28** 4703105
[37] Teyber R, Marchevsky M, Prestemon S, Weiss J and van der Laan D 2020 *Supercond. Sci. Technol.* **33** 095009
[38] Tixador P, Nguyen-Nhat T, Okada-Vieira H and Ponceau R 2010 *IEEE Trans. Appl. Supercond.* **21** 1194–7
[39] Zampa A, Lacroix C, Badel A, Sirois F and Tixador P 2022 *Supercond. Sci. Technol.* **35** 095003
[40] Lacroix C and Sirois F 2014 *Supercond. Sci. Technol.* **27** 035003
[41] Lacroix C, Lapierre Y, Coulombe J and Sirois F 2014 *Supercond. Sci. Technol.* **27** 055013
[42] Saad H B, Horn-Bourque D, Hartman S M B, Errabie H, Lacroix C and Sirois F 2024 *IEEE Trans. Appl. Supercond.* **35** 6600210
[43] Superpower (available at: www.superpower-inc.com/specification.aspx) (Accessed on June 2021)
[44] Ekin J 2006 *Experimental Techniques for low-Temperature Measurements: Cryostat Design, Material Properties and Superconductor Critical-Current Testing* (Oxford University Press)
[45] Bagrets N, Nast R, Fournier-Lupien J H, Sirois F, Celentano G and Weiss K P 2021 *IEEE Trans. Appl. Supercond.* **31** 1–8
[46] Russek S E, Sanders S, Roshko A and Ekin J 1994 *Appl. Phys. Lett.* **64** 3649–51
[47] Barusco P, Ben-Saad H, Horn-Bourque D, Lacroix C, Sirois F, Puig T, Gutiérrez J, Granados X and Obradors X 2024 *IEEE Trans. Appl. Supercond.* **34** 6600906
[48] Canavan E R, Leidecker H and Panashchenko L 2015 Conductance degradation in HTS coated conductor solder joints *IOP Conf. Ser.: Mater. Sci. Eng.* 102 012032
[49] Barth C, Van Der Laan D, Bagrets N, Bayer C M, Weiss K P and Lange C 2015 *Supercond. Sci. Technol.* **28** 065007
[50] Weiss J D, Kim C, Pamidi S and van der Laan D C 2019 *Supercond. Sci. Technol.* **32** 034005
[51] Willering G, Van Der Laan D, Weijers H, Noyes P, Miller G and Viouchkov Y 2015 *Supercond. Sci. Technol.* **28** 035001
[52] Majoros M, Sumption M, Collings E and Van Der Laan D 2016 *Supercond. Sci. Technol.* **29** 044006
[53] Laan D, Radcliff K, Anvar V, Wang K, Nijhuis A and Weiss J 2021 *Supercond. Sci. Technol.* **34** 10LT01
[54] Bonura M and Senatore C 2016 *IEEE Trans. Appl. Supercond.* **27** 6600705
[55] Van Nugteren J, Dhallé M, Wessel S, Krooshoop E, Nijhuis A and Ten Kate H 2015 *Phys. Proc.* **67** 945–51